Nonlinear Zeeman splitting of magnetoexcitons in *c*-plane wurtzite GaN-based quantum wells

W. Bardyszewski
Faculty of Physics, University of Warsaw, ul. Hoża 69, 00-681 Warszawa, Poland

S. P. Łepkowski
Institute of High Pressure Physics, "Unipress", Polish Academy of Sciences, ul. Sokołowska 29/37, 01-142 Warszawa, Poland
(Received 2 April 2014; revised manuscript received 16 July 2014; published 8 August 2014)

We present a theoretical description of excitonic spectra in GaN-based quantum wells in a wide range of magnetic fields taking into account built-in strain and electric fields, and valence band mixing due to the quantum well confinement. Our calculations performed for the GaN/AlGaN quantum wells reveal a nonlinear behavior of the excitonic Zeeman splitting on magnetic field. We have determined that the low magnetic field g-factor dependence on the quantum well width shows a steplike variation due to the reordering of the light- and heavy-hole valence subbands. Sharp change of the g factor is also predicted for InGaN/GaN quantum wells grown on a virtual metamorphic InGaN substrate.

DOI: 10.1103/PhysRevB.90.075302 PACS number(s): 78.67.De, 71.35.Ji, 78.55.Cr

I. INTRODUCTION

Optical experiments in strong magnetic field provide valuable information concerning electronic properties of semiconductor structures. One of the most important parameters determining the shape of the optical spectra in the magnetic field is the effective g factor, which is responsible for the Zeeman splitting of spectral lines. Measuring this splitting leads to better understanding of the symmetry of the electronic states participating in the optical transitions. In the simplest approximation the excitonic g factor is equal to the difference of the g factors of electrons in the conductance and valence bands. However, this point of view turned out to be oversimplified, especially in the case of semiconductor heterostructures characterized by strong confinement of electrons such as widely studied GaAs/AlGaAs quantum wells (QWs). Using different experimental techniques it was observed that the Zeeman splitting of so-called heavy-hole excitons departs from linearity and even changes sign when the QW becomes wide enough [1–5]. This phenomenon is attributed to the mixing between light- and heavy-hole states in the valence subbands [2]. Two basic mechanisms were identified, which could contribute to the subband mixing in excitons, namely the $k \cdot p$ perturbation and the electron-hole Coulomb coupling. Nonlinear splitting of excitons in the magnetic field was also found in InGaAs/GaAs QWs [3].

Properties of magnetoexcitons are much less studied in the case of group III-nitride semiconductors. So far, there are only few reports on this subject. It has been observed that in the case of bulk GaN, the Zeeman splitting of the optically active A exciton in the magnetic field parallel to the crystalline c axis is approximately equal to zero [6]. This information was subsequently used to estimate the so-called Luttinger valence band parameter κ for both excitonic [6,7] and bare, one-particle valence band states [8]. The striking difference in obtained values of κ in both cases was attributed to strong mixing of the various valence band sublevels due to the $k \cdot p$ and Coulomb interaction [8]. Subband mixing can become even more pronounced in GaN-based QWs due to built-in strain arising from the lattice mismatch between barriers and QWs, and strong built-in electric field caused by the spontaneous and piezoelectric polarizations, which influences the subbands due to the quantum-confinement Stark effect.

Consequently, the behavior of such structures in the magnetic field may depart significantly from the bulk materials. In particular, as it was established experimentally [9], the excitonic g factor in narrow GaN/AlGaN QWs may take values as high as 3.5. It was also demonstrated that increasing the QW width reduces its value to about 2. This phenomenon was interpreted as being caused by the reordering of the valence subbands with different symmetries. It has been further proposed that the higher value of the g factor corresponds to the configuration in which the topmost valence band is of Γ_7 symmetry [termed as light-hole (LH) like] and that the reduction of the g factor occurs when the topmost valence subband is of Γ_9 symmetry [heavy-hole (HH) like]. The proper description of this effect requires inclusion both $k \cdot p$ mixing of subbands and Coulomb interaction between the electron and the hole, i.e., excitonic effects.

The well established model of magnetoexcitons in QWs made of zinc-blend structure semiconductors such as GaAs/AlGaAs was proposed in the 1980s [10]. Magnetoexcitons in bulk wurtzite GaN in the limit of weak magnetic field were theoretically discussed in Ref. [7] and subsequently, for the case of arbitrary strong field in Ref. [8]. In this work we present a theoretical description of excitonic spectra in GaN-based QWs in a wide range of magnetic fields taking into account mixing between the valence subbands. We show that our model is well suited for interpretation of the optical g-factor measurements in c-plane GaN/AlGaN QW structures in the magnetic field parallel to the QW growth axis. This model also predicts unusual dependence of the g factor in InGaN/GaN QWs with tensile strained barriers.

II. THEORETICAL MODEL

In order to describe the excitonic optical spectra of QW systems within the framework of the Kubo linear response theory, we consider the retarded momentum-momentum Green's

function:

$$\Pi(t) = -i\Theta(t) < [\hat{P}_\varepsilon(t), \hat{P}^\dagger_\varepsilon(0)]_- >= -i\sum_{1,2} P^\varepsilon_{2,1}\Psi_{1,2}(t), \tag{1}$$

where we have introduced the time-dependent exciton wave function: $\Psi_{1,2} = \Theta(t) < [a^\dagger_2(t)a_1(t), \hat{P}^\dagger_\varepsilon(0)]_- >$. The angular and square brackets represent ensemble averaging and commutator, respectively. Here $\hat{a}^\dagger_1$ and $\hat{a}_2$ are creation and annihilation operators for electron band states 1 and 2, respectively. In our convention the indices 1 denote single electron conduction bands states and the indices 2 denote the states in the valence bands. The interband part of the momentum operator responsible for promoting electrons from the valence band to the conduction band is defined by $\hat{P}^\dagger_\varepsilon(t) = \sum_{1,2} P^\varepsilon_{1,2}a^\dagger_1(t)a_2(t)$, where $P^\varepsilon_{1,2} = \langle 1|\vec{\varepsilon}\cdot\hat{\vec{p}}|2\rangle$ is equal to the interband momentum matrix element for the polarization vector of light $\vec{\varepsilon}$.

The time evolution of the exciton wave function is governed by the Bethe-Salpeter equation:

$$\begin{aligned} i\hbar\frac{\partial}{\partial t}\Psi_{1,2}(t) &= \sum_{\bar{1},\bar{2}}\left[\mathcal{H}^C_{1\bar{1}}\delta_{2\bar{2}} - \bar{\mathcal{H}}^V_{2\bar{2}}\delta_{1\bar{1}}\right]\Psi_{\bar{1},\bar{2}}(t) \\ &\quad - \sum_{\bar{2},\bar{1}} V_{1,\bar{2},2,\bar{1}}\Psi_{\bar{1},\bar{2}}(t) + i\hbar\delta(t)P^\varepsilon_{1,2} \\ &\equiv \sum_{\bar{1},\bar{2}}\mathcal{H}^X_{12,\bar{1}\bar{2}}\Psi_{\bar{1},\bar{2}}(t) + i\hbar\delta(t)P^\varepsilon_{1,2}. \end{aligned} \tag{2}$$

Here single-particle Hamiltonian matrices for the conduction and valence band states are denoted by $\mathcal{H}^C_{1\bar{1}}$ and $\mathcal{H}^V_{2\bar{2}}$, respectively, and the $V_{1,\bar{2},2,\bar{1}}$ matrix elements describe both direct and exchange electron-hole Coulomb interaction. Note that the valence band part of the exciton Hamiltonian, $\bar{\mathcal{H}}^V_{2\bar{2}}$ matrix, is equal to the complex conjugate of the valence band Hamiltonian $\mathcal{H}^V_{2\bar{2}}$. This expression has the form of the Schrödinger equation with the effective exciton Hamiltonian $\mathcal{H}^X_{12,\bar{1}\bar{2}}$ and with the initial condition $\Psi_{\bar{1},\bar{2}}(0) = P^\varepsilon_{1,2}$. Its solution can be expanded in terms of the eigenstates of $\mathcal{H}^X_{12,\bar{1}\bar{2}}$ as:

$$\Psi_{1,2}(t) = \sum_\lambda e^{-\frac{i}{\hbar}E^X_\lambda t}\langle\Psi^\lambda|P^\varepsilon\rangle\Psi^\lambda, \tag{3}$$

where the eigenstates Ψ^λ and the eigenenergies E^X_λ are obtained from the eigenequation [11,12]:

$$\mathcal{H}^X\Psi^\lambda = E^X_\lambda\Psi^\lambda. \tag{4}$$

The absorption coefficient is proportional to the imaginary part of the Fourier transform of $\Pi(t)$ [Eq. (1)] and it can be expressed in terms of the exciton eigenstates, Eq. (4), as:

$$\alpha(\omega) = \frac{4\pi e^2}{cn_r m_0^2\hbar\omega L_W\mathcal{A}}\sum_\lambda |\langle P^\varepsilon|\Psi^\lambda\rangle|^2\delta\left(\omega - E^X_\lambda/\hbar\right), \tag{5}$$

where L_W and $\mathcal{A}$ are the QW width and area, respectively; n_r, the refractive index; m_0, the electron mass; $e > 0$, the elementary charge. The transition energies are therefore equal to the excitonic eigenenergies E^X_λ, while the line intensities are proportional to $|\langle P^\varepsilon|\Psi^\lambda\rangle|^2$, squared overlaps of the exciton eigenfunctions with the initial state $|P^\varepsilon\rangle$.

Considering the structure of the valence and conduction bands in wurtzite nitrides we take into account the spin-degenerate s-type conduction band of Γ_7 symmetry and three p-type double degenerate valence bands, which are split by the spin orbit and crystal field interactions. By assumption, the magnetic field $\vec{B}$ is directed along the z axis, parallel to the crystalline c axis and perpendicular to the QW plane. The kinetic momenta of the electron and hole are given by $\vec{p}_1 = -i\hbar\vec{\nabla}_1 + \frac{e}{c}\vec{A}(\vec{r}_1)$ and $\vec{p}_2 = i\hbar\vec{\nabla}_2 + \frac{e}{c}\vec{A}(\vec{r}_2)$, respectively with the vector potential assumed in the symmetric gauge $\vec{A}(\vec{r}) = \frac{1}{2}\vec{r}\times\vec{B}$. According to our notation $\vec{r}_1$ and $\vec{r}_2$ denote positions of the electron and of the hole, respectively. The effective exciton Hamiltonian constructed within the effective mass approximation, using the same basis set as in Ref. [13] has the form:

$$\begin{aligned} \mathcal{H}^X(\vec{p}_1,\vec{p}_2) &= \left(\frac{p^2_{1z}}{2m_z} + \frac{p^2_{1\perp}}{2m_\perp} + g_0\mu_B B_z\sigma_c + E_g + U_c - U_v - \frac{e^2}{\epsilon|\vec{r}_1 - \vec{r}_2|}\right)\hat{I}_{6\times6} - \Delta_2\hat{\sigma}_z\otimes\hat{J}_z - \sqrt{2}\Delta_3(\hat{\sigma}_-\otimes\hat{J}_+ + \hat{\sigma}_+\otimes\hat{J}_-) \\ &\quad - \hat{\sigma}_0\otimes\left(\Delta_1\hat{J}^2_z + \left(A_1\hat{I}_{3\times3} + A_3\hat{J}^2_z\right)p^2_{2\,z} + \left(A_2\hat{I}_{3\times3} + A_4\hat{J}^2_z\right)\left(p^2_{2\,x} + p^2_{2\,y}\right) - A_5\left(\hat{J}^2_+p^2_{2\,-} + \hat{J}^2_-p^2_{2\,+}\right)\right. \\ &\quad \left. - 2A_6p_{2\,z}([\hat{J}_z,\hat{J}_+]_+p_{2\,-} + [\hat{J}_z,\hat{J}_-]_+p_{2\,+}) - \mu_B(3\kappa+1)B_z\hat{J}_z\right) - \frac{1}{2}g_0\mu_B B_z\hat{\sigma}_z\otimes\hat{I}_{3\times3} + \mathcal{H}^{\text{strain}}, \end{aligned} \tag{6}$$

where

$$\begin{aligned} \mathcal{H}^{\text{strain}} &= -\hat{\sigma}_0\otimes\left\{\left[D_1\hat{I}_{3\times3} + D_3\hat{J}^2_z\right]\varepsilon_{zz}(z_2) + \left(D_2\hat{I}_{3\times3} + D_4\hat{J}^2_z\right)[\varepsilon_{xx}(z_2) + \varepsilon_{yy}(z_2)]\right\} \\ &\quad + \hat{I}_{6\times6}\{a_{cz}\varepsilon_{zz}(z_1) + a_{c\perp}[\varepsilon_{xx}(z_1) + \varepsilon_{yy}(z_1)]\}. \end{aligned}$$

This form of the strain Hamiltonian is appropriate for the biaxial stress in the plane perpendicular to the c-axis. The strain tensor values in the given layer of a multi-QW structure are equal to $\epsilon_{xx,\text{layer}} = \epsilon_{yy,\text{layer}} = \frac{a_{\text{substrate}}}{a_{\text{layer}}} - 1$ and $\epsilon_{zz,\text{layer}} = -\frac{2C_{13}}{C_{33}}\epsilon_{xx,\text{layer}}$, where C_{13} and C_{33} denote the elastic constants in the layer.

In the following, we label the valence band states by quantum numbers, such as spin σ_v or angular momentum J_z, pertinent to electrons (electron representation). The exchange interaction, which is rather small in nitrides, is treated as a perturbation, so in the first-order approximation, the projection of the conduction electron on the z axis denoted as σ_c is a

good quantum number for the excitonic eigenstates [13]. The 3×3 matrices $\hat{J}_{x,y,z}$ represent the components of the angular momentum operator with $J = 1$. Furthermore, $\hat{J}_{\pm} = \frac{1}{\sqrt{2}}(\hat{J}_x \pm i\hat{J}_y)$, $p_{2\pm} = p_{2x} \pm ip_{2y}$ and $\hat{\sigma}_{\pm} = \frac{1}{2}(\hat{\sigma}_x \pm i\hat{\sigma}_y)$, where $\hat{\sigma}_{x,y,z}$ are standard Pauli matrices referring in our representation to the spin of valence band electrons. The square brackets denote the symmetrized product $[\hat{J}_z, \hat{J}_{\pm}]_+ = \frac{1}{2}(\hat{J}_z\hat{J}_{\pm} + \hat{J}_{\pm}\hat{J}_z)$. The basis set for the electron states in the conduction and valence bands and the matrices $\hat{J}_{x,y,z}$ in this representation are taken from Ref. [14]. The terms proportional to the $B_z\hat{\sigma}_z$ and $B_z\hat{J}_z$ describe the coupling of the valence electron spin and angular momentum with the magnetic field. The Hamiltonian is parametrized with valence band parameters $A_{1,\ldots,6}$, $\Delta_{1,2,3}$, the conduction band effective masses, m_z,$m_{\perp}$ and the energy gap, E_g. The Luttinger coupling constant of the valence band electrons to the magnetic field is denoted by κ and the effective g factors for electrons in the valence and conduction bands are assumed to be equal to $g_0 = 2$. The electron-hole interaction is described by the Coulomb potential screened with the isotropic dielectric constant ε. The strain-dependent part of the Hamiltonian is parametrized with valence band deformation potentials $D_{1,\ldots,4}$ and conduction band deformation potentials a_{cz} and $a_{c\perp}$. The potential profiles of the conduction and the valence bands, in the QW structure are defined as:

$$U_c(z) = U_{0c} + eE_z z \quad U_v(z) = U_{0v} + eE_z z, \tag{7}$$

where the U_{0c} and U_{0v} denote the energy of the band edges in unstrained material in the conduction and the valence band, respectively. The built-in electric field E_z is different in the QW and barrier region and is obtained from:

$$E_W = \frac{L_B(P_{\mathrm{tot},B} - P_{\mathrm{tot},W})}{L_W\lambda_B + L_B\lambda_W}, \qquad E_B = -\frac{L_W}{L_B}E_W, \tag{8}$$

where L_W and L_B denote the widths of the QW and the barriers, and λ is the electric permittivity of the corresponding material [15]. The total electric polarization including the first and the second-order piezoelectric effects and the spontaneous polarization is given by:

$$\begin{aligned} P_{\mathrm{tot},W} = {} & P_{sp,W} + 2e_{31,W}\epsilon_{xx,W} + e_{33,W}\epsilon_{zz,W} + e_{311,W}\epsilon^2_{xx,W} \\ & + e_{333,W}\epsilon^2_{zz,W} + e_{133,W}\epsilon_{xx,W}\epsilon_{zz,W}, \end{aligned} \tag{9}$$

where the values of the spontaneous polarization P_{sp} and the piezoelectric coefficients e_{ij} and e_{ijk} are determined in Ref. [16].

In order to diagonalize the excitonic Hamiltonian in the QW in the magnetic field, it is convenient to separate the motion in the z direction (perpendicular to the QW plane) and the relative motion of the electron and hole in the QW plane. The motion in the z direction is described using the envelope functions $F^C_{m,M}$ and $F^V_{n,N}$, which are obtained by diagonalizing the conduction and valence band Hamiltonians at the two-dimensional Brillouin zone center. The motion of the electron and hole in the QW plane is described using the set of center-of-mass $\vec{R}_{\perp} = (\vec{r}_{1\perp} + \vec{r}_{2\perp})/2$ and relative coordinates $\vec{r}_{\perp} = \vec{r}_{1\perp} - \vec{r}_{2\perp} = x\hat{i} + y\hat{j}$, and corresponding momenta $\vec{P}_{\perp} = \vec{p}_{1\perp} + \vec{p}_{2\perp}$ and $\vec{p}_{\perp} = (\vec{p}_{1\perp} - \vec{p}_{2\perp})/2$. By applying the Lamb gauge transformation [17] and restricting only to the states with zero center-of-mass momentum $\vec{P}_{\perp} = \vec{0}$, this transformation amounts to substitution: $\vec{p}_{1\perp} \to \vec{\pi}_a$ and $\vec{p}_{2\perp} \to \vec{\pi}_b$ in the Hamiltonian Eq. (6), where $\vec{\pi}_a = -i\hbar\vec{\nabla}_{r_{\perp}} + \frac{e}{c}\vec{A}(\vec{r}_{\perp})$ and $\vec{\pi}_b = -i\hbar\vec{\nabla}_{r_{\perp}} - \frac{e}{c}\vec{A}(\vec{r}_{\perp})$ refer only to the relative position $\vec{r}_{\perp}$.

Due to the axial symmetry of the exciton Hamiltonian, the total angular momentum in the z direction, L_z is conserved. The value of L_z is determined by the polarization of incident light and may take values $L_z = \pm 1$ for circular polarizations of light $\sigma_{\pm}$, and $L_z = 0$ for the linear polarization σ_z along the z axis. In order to diagonalize the exciton Hamiltonian (6) we introduce the symmetrized basis set to describe the electron-hole pair states with fixed values of L_z and σ_c:

$$\begin{aligned} \Phi^{L_z}_{sMN\sigma_c}(\vec{r}_{\perp},z_1,z_2) = {} & \sum_{n=0}^{\infty}\sum_{J_z,\sigma_v}\varphi_{ns}(\vec{r}_{\perp})F^C_{\sigma_c,M}(z_1)\bar{F}^V_{J_z\sigma_v,N}(z_2) \\ & \times |C,\sigma_c\rangle\hat{\mathcal{K}}|V,J_z\sigma_v\rangle\delta_{L_z,n-s+\sigma_c-J_z-\sigma_v}. \end{aligned} \tag{10}$$

Here $F^C_{\sigma_c,M}(z_1)$ and $F^V_{J_z\sigma_v,N}(z_2)$ denote the conduction and valence band envelope functions obtained for $p_{\perp} = 0$ and $B = 0$. They are labeled by M and N, respectively. The bulk zone-center states $|C,\sigma\rangle$ and $|V,J_z,\sigma_v\rangle$ are defined in Ref. [13] and the time reversal operator $\hat{\mathcal{K}}$ reflects the symmetry of hole states with respect to electron states. The relative motion of the electron and hole in the QW plane is expressed using the Landau orbitals $\varphi_{ns}(\vec{r}_{\perp})$.

According to the definition of the Landau orbitals:

$$\varphi_{ns}(\vec{r}_{\perp}) = \frac{(\hat{a}_0^{\dagger})^n(\hat{b}_0^{\dagger})^s}{l_0\sqrt{2\pi n!s!}}\exp\left(-\frac{r_{\perp}^2}{4l_0^2}\right), \tag{11}$$

their spatial extension is determined by the magnetic length $l_0 = \sqrt{\hbar/eB_0}$ associated with the fictitious magnetic field $\vec{B}_0$. The magnitude of $\vec{B}_0$ is adjusted in order to optimize the results of calculations of the exciton ground state. We have checked that the best results are obtained when l_0 is comparable with the exciton radius, which in the case of GaN-based QWs corresponds to $B_0 = 15$T.

Landau orbitals are generated using the ladder operators $\hat{a}_0^{\dagger}$ and $\hat{b}_0^{\dagger}$:

$$\begin{aligned} \hat{a}_0^{\dagger} &= \frac{1}{\sqrt{2}}\left[-l_0\left(\frac{\partial}{\partial x} + i\frac{\partial}{\partial y}\right) + \frac{1}{2l_0}(x + iy)\right], \\ \hat{b}_0^{\dagger} &= \frac{1}{\sqrt{2}}\left[-l_0\left(\frac{\partial}{\partial x} - i\frac{\partial}{\partial y}\right) + \frac{1}{2l_0}(x - iy)\right]. \end{aligned} \tag{12}$$

Each $\varphi_{ns}(\vec{r}_{\perp})$ has a well-defined z component of the angular momentum equal to $\hbar(n - s)$. Due to the Kronecker δ function $\delta_{L_z,n-s+\sigma_c-J_z-\sigma_v}$ the sum in Eq. (10) is restricted to terms with fixed total angular momentum in the z direction equal to L_z.

Operators of relative electron-hole momentum in the QW plane are expressed in terms of the ladder operators in the following way:

$$\begin{aligned} \pi_{a+} = \pi_{ax} + i\pi_{ay} &= \frac{i\hbar}{\sqrt{2}l}\left[\left(\frac{l_0}{l} + \frac{l}{l_0}\right)\hat{a}_0^{\dagger} + \left(\frac{l_0}{l} - \frac{l}{l_0}\right)\hat{b}_0\right] \\ \pi_{b+} = \pi_{bx} + i\pi_{by} &= -\frac{i\hbar}{\sqrt{2}l}\left[\left(\frac{l_0}{l} + \frac{l}{l_0}\right)\hat{b}_0 + \left(\frac{l_0}{l} - \frac{l}{l_0}\right)\hat{a}_0^{\dagger}\right], \end{aligned} \tag{13}$$

where l is equal to the magnetic length corresponding to the actual magnetic field value B.

The excitonic eigenstates are obtained as the linear combinations of the basis functions:

$$\Psi^{\lambda}(\vec{r}_{\perp},z_1,z_2)=\sum_{sMN\sigma_c}\psi^{\lambda}_{sMN\sigma_c}\Phi^{L_z}_{sMN\sigma_c}(\vec{r}_{\perp},z_1,z_2). \quad (14)$$

The coefficients $\psi^{\lambda}_{sMN\sigma_c}$ and the exciton eigenenergies E^X_{λ} are determined by diagonalizing the Hamiltonian (6) using the Lanczos reduction method with $|P^{\varepsilon}\rangle$ as an initial vector. The exciton Hamiltonian has axial symmetry and for the circular polarization of light in the xy plane, the vector $|P^{\varepsilon}\rangle$ has a definite z component of angular momentum. Thus the Lanczos procedure generates only states with prescribed symmetry with nonvanishing scalar product $\langle P^{\varepsilon}|\Psi^{\lambda}\rangle$. Consequently, we have found that quite accurate description of the exciton spectra could be obtained using the Lanczos basis set not exceeding 300 vectors, given the original dimension of the problem equal to a few thousands.

The overlaps of the exciton eigenfunctions with the initial-state vector determining the intensity of the excitonic lines in Eq. (5) are given by

$$\langle P^{\varepsilon}|\Psi^{\lambda}\rangle=\sum_{sMN\sigma_c}\bar{P}^{\varepsilon}_{MN\sigma_c}\psi^{\lambda}_{sMN\sigma_c} \quad (15)$$

with

$$P^{\varepsilon}_{MN\sigma_c}=\frac{\mp 1}{\sqrt{2\pi}l_0}P_{CV}\int dz\, F^{C}_{\sigma_c,M}(z)\bar{F}^{V}_{-L_z\sigma_c,N}(z), \quad (16)$$

where $P_{CV}=\langle iS|\frac{\hbar}{i}\frac{\partial}{\partial x}|X\rangle=\frac{m_0}{\hbar}P_2$ denotes the bulk interband momentum matrix element, which is related to the Kane's parameter P_2 [14]. The upper sign corresponds to $L_z=1$ for circular light polarization σ_+, while the lower sign corresponds to $L_z=-1$ for circular polarization σ_-, respectively.

III. RESULTS AND DISCUSSION

Our model is now applied to study the excitonic g factor in c plane GaN/Al_xGa_{1-x}N QWs grown on GaN substrate and In_xGa_{1-x}N/GaN QWs grown on In_yGa_{1-y}N buffer layer with $y<x$. In both cases tensile strain is present in the barriers, so that the highest valence level has light-hole symmetry in narrow QWs. We focus on GaN/AlGaN QWs for which experimental data were obtained for the wide range of magnetic fields up 55 T [9]. As suggested in the previous section, the calculations are preformed in two steps. First, we obtain the envelope functions for electron and hole states in the QW structures in the center of the Brillouin zone at zero magnetic field. In the next step, the excitonic Hamiltonian for the given magnetic field is diagonalized using the basis set constructed from those envelope functions according to Eq. (10). The calculations are performed for σ_+ and σ_- circular polarizations of light with respect to the c axis, in the range of the magnetic fields between 0 T and 55 T. The $k\cdot p$ Hamiltonian parameters for the conduction and valence bands in GaN, AlN and InN are estimated from the recent quasiparticle self-consistent GW band structure calculations in Ref. [18], while the elastic constants for those materials are taken from Ref. [15]. The parameters for Al_xGa_{1-x}N and In_xGa_{1-x}N alloys are obtained using the linear interpolation between binaries except for the energy gap, the spontaneous polarization, and the piezoelectric constants for which the bowing is taken into account as in Refs. [15] and [16].

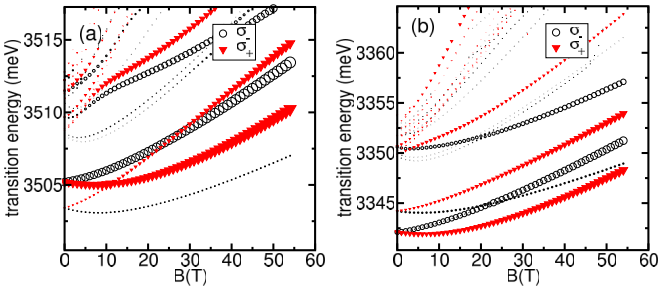

FIG. 1. (Color online) Excitonic transition energies and intensities as functions of the magnetic field in two GaN/$Al_{0.1}Ga_{0.9}$N QW structures with L_W equal to 1.5 nm (a) and 4 nm (b) and $L_B=150$ nm for two circular polarizations of light. The relative intensities of absorption lines are represented by the size of corresponding symbols.

In Fig. 1, we present the influence of the magnetic field on the excitonic transition energies and intensities in two GaN/$Al_{0.1}Ga_{0.9}$N QW structures with L_W equal to 1.5 nm and 4 nm and $L_B=150$ nm, which were obtained for two different circular polarizations of light. The relative intensities of absorption transitions are represented by the size of corresponding symbols. The spectrum for the narrow QW in Fig. 1(a) shows that the lowest-energy transition line corresponds to the light-hole or B exciton. It is split with the magnetic field in such a way that the transition with σ_- polarization occurs at lower energy than the transition with σ_+ polarization of light. The next transition line corresponding to the heavy-hole or A exciton is split in the opposite sense, i.e., the transition with σ_+ polarization has lower energy than the σ_- transition. For wider QW with $L_W=4$ nm the relative positions of A and B excitonic transitions are interchanged as illustrated in Fig. 1(b), and the intensity of the transition line with lower energy is larger than the intensity of the higher-energy line. In both cases the intensity of A-exciton lines is about 10 times larger than the intensity of the B-exciton lines at zero magnetic field. With increasing magnetic field the transition strength is increasing for both heavy- and light-hole excitons. The fastest growth of transition intensity is observed in the case of the B exciton in the σ_+ polarization.

Since we are interested in the excitonic g factor obtained from the analysis of the photoluminescence spectra, we focus on the lowest-energy transition lines as functions of the magnetic field. In Fig. 2(a), the energy splitting between the transitions with polarizations σ_+ and σ_- for two QW widths $L_W=1.5$ nm and $L_W=4$ nm are presented. In the first case the lowest-energy transition corresponds to the light-hole exciton and the energy splitting is positive, while in the other case the lowest-energy transition is attributed to the heavy-hole exciton and the energy splitting has the opposite sign. It is interesting to note that the splitting is not linear as a function of the magnetic field. The deviation from linearity is more apparent in the case of the wider QW. The effective g factors derived from the Zeeman splittings shown in Fig. 2(a) are plotted in Fig. 2(b). For both heavy- and light-hole excitons a significant reduction of the magnitude of the g factor with

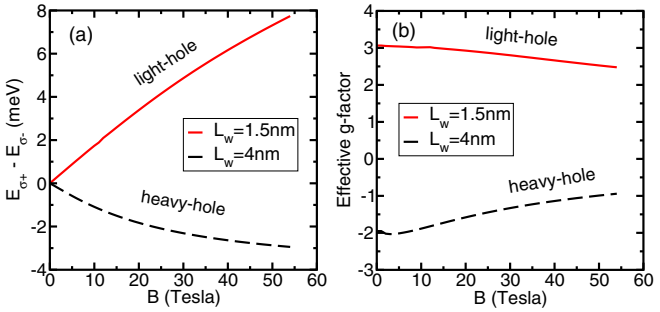

FIG. 2. (Color online) Magnetic field dependence of the energy splitting between the lowest-energy transitions with polarizations σ_+ and σ_- (a) and the corresponding effective g factors (b) in two GaN/$Al_{0.1}Ga_{0.9}$N QWs with QW widths $L_W = 1.5$ nm (solid line) and $L_W = 4$ nm (dashed line).

the magnetic field is observed. Nevertheless, we may define the low magnetic field g factor as half of the slope of curves in Fig. 2(a) at $B = 0$T. In order to make connection to the experimental results presented in Ref. [9], we have evaluated the g factor for several GaN/Al_xGa_{1-x}N QW structures grown on GaN substrates.

In Fig. 3 we present the dependence of the absolute value of the low magnetic field g factor on the QW width, L_W, in GaN/Al_xGa_{1-x}N QWs with three barrier thicknesses, L_B, and Al content $x = 0.1$ [Fig. 3(a)] and $x = 0.15$ [Fig. 3(b)]. In agreement with the experimental observations in Ref. [9], the absolute value of the g factor decreases with the QW width from about $|g| = 3.5$ for $L_W = 1$ nm wide QW to about $|g| = 2$ for wider QWs. The transition from the high to low value of the g factor as a function of QW width has almost a steplike character and depends on the barrier thickness L_B. The sharp drop of the g factor is associated with the reordering of the excitonic transitions A and B as illustrated in Fig. 4 for the specific case of the QW barrier $L_B = 100$ nm and the Al composition in the barrier $x = 0.1$. Note that the excitonic transition energy crossing ($E_{\Gamma_9} - E_{\Gamma_7} = 0$) in this case corresponds exactly to the QW width at which the absolute value of the g factor drops from the value 3.5 to about 2 [Fig. 3(a)]. At the same time it is interesting to note

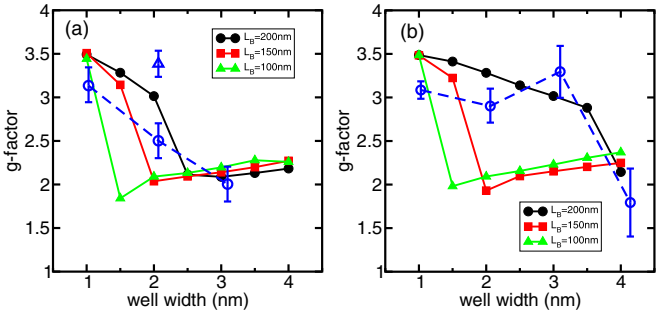

FIG. 3. (Color online) The dependence of the absolute value of the low magnetic field g factor on the QW width L_W for three barrier thicknesses L_B in GaN/Al_xGa_{1-x}N QWs with Al content $x = 0.1$ (a) and Al content $x = 0.15$ (b). The experimental points (open symbols) from Ref. [9] for QWs with $x = 0.08$ and $x = 0.13$ are inserted in figures (a) and (b), respectively.

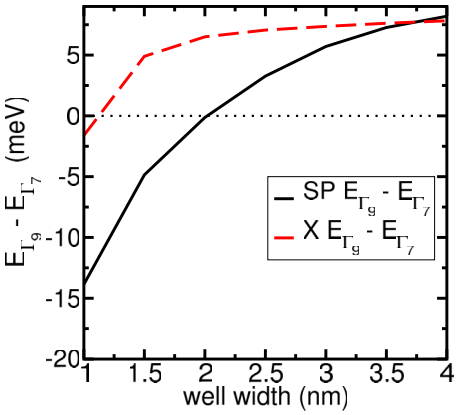

FIG. 4. (Color online) Valence band single-particle (SP) energy difference $E_{\Gamma_9} - E_{\Gamma_7}$ (solid line) and difference in excitonic transition energies (X) from the Γ_7 and Γ_9 valence band states to the conduction band in GaN/$Al_{0.1}Ga_{0.9}$N QW with barrier $L_B = 100$ nm as functions of QW width.

that the single-particle transition energy crossing, i.e., when the excitonic effect are neglected, occurs at significantly wider QWs.

The energy crossing of the HH and LH levels in the valence band is accompanied with the dramatic change of the shape of the topmost level envelope function as illustrated in Fig. 5. In the case of narrow GaN/$Al_{0.1}Ga_{0.9}$N QW with $L_w = 1$ nm the topmost valence level is of Γ_7 symmetry (LH) and the corresponding envelope function penetrates into the barrier more deeply than in the case of wider, $L_w = 4$ nm QW with Γ_9 (HH) level at the top of the valence band. The overlap between the conduction and valence band envelope functions is therefore much smaller in the former case, which leads to the reduction of the optical transition intensity for B excitons compared to the A excitons as shown in Fig. 1.

Steplike variation of the g factor with the QW width can be also observed in In_xGa_{1-x}N/GaN QWs with tensile strained barriers grown on In_yGa_{1-y}N metamorphic layer as a virtual substrate [19,20]. Figure 6(a) shows the QW width dependence of the absolute value of the low magnetic field g factor in such structures for the barrier thickness $L_B = 20$ nm and In content in the QW and substrate equal to $x = 0.15$ and $y = 0.1$,

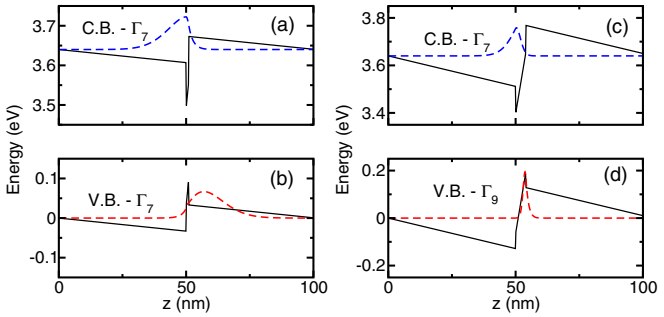

FIG. 5. (Color online) (a) The square root of the electron probability density in the lowest conduction and the topmost valence subbands in GaN/$Al_{0.1}Ga_{0.9}$N QWs structures with $L_w = 1$ nm (a)–(b) and $L_w = 4$ nm (c)–(d), respectively for the barrier width $L_B = 100$ nm.

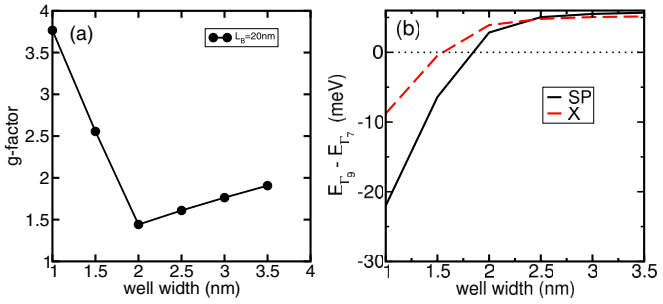

FIG. 6. (Color online) (a) Dependence of the absolute value of the low magnetic field g factor in $In_{0.15}Ga_{0.85}N/GaN$ QWs with barriers of thickness $L_B = 20$ nm grown on $In_{0.1}Ga_{0.9}N$ metamorphic layer. (b) Valence band single-particle (SP) energy difference $E_{\Gamma_9} - E_{\Gamma_7}$ (solid line) and difference in excitonic transition energies from the Γ_7 and Γ_9 valence band states to the conduction band for the same structures as in (a).

respectively. The sharp change of the g factor is again caused by the reordering of excitonic transitions related to heavy- and light-hole subbands. In Fig. 6(b), we show the energy difference for transitions to the conduction band from the topmost valence band levels of symmetry Γ_9 and Γ_7 without excitonic effects and including excitonic effect as function of QW width. Similarly as in GaN/AlGaN QW (Fig. 4), the crossing of the excitonic transition energies occurs at smaller QW widths than in the case of single-particle transitions.

IV. CONCLUSIONS

In conclusion we have developed a model of excitonic transitions in c-plane wurtzite QWs applicable for a wide range of magnetic fields. By including the built-in strain, the internal electric field, the valence band mixing due to the QW confinement and Coulomb interaction, we were able to describe properly the dependence of the optical transition energies on the magnetic field. Our calculations performed for GaN/AlGaN QWs have revealed a nonlinear magnetic field dependence of the excitonic Zeeman splitting on the magnetic field, which leads to the significant reduction of the effective g factor with the magnetic field. We have also shown that the absolute value of the low field g factor changes in a steplike fashion as function of QW width in agreement with the experimental results reported in Ref. [9]. Sharp change of the g factor is also predicted for InGaN/GaN QWs grown on a virtual metamorphic InGaN substrate.

ACKNOWLEDGMENTS

This work was supported by the Polish National Science Center, Project No. 2012/07/B/ST3/03174.

[1] W. Ossau, B. Jäkel, E. Bangert, G. Landwehr, and G. Weimann, Surf. Sci. **174**, 188 (1986).
[2] G. E. W. Bauer and T. Ando, Phys. Rev. B **37**, 3130(R) (1988).
[3] N. J. Traynor, R. J. Warburton, M. J. Snelling, and R. T. Harley, Phys. Rev. B **55**, 15701 (1997).
[4] S. Glasberg, G. Finkelstein, H. Shtrikman, and I. Bar-Joseph, Phys. Rev. B **59**, R10425 (1999).
[5] J. Jadczak, M. Kubisa, K. Ryczko, L. Bryja, and M. Potemski, Phys. Rev. B **86**, 245401 (2012).
[6] R. Stepniewski, M. Potemski, A. Wysmolek, K. Pakula, J. M. Baranowski, J. Lusakowski, I. Grzegory, S. Porowski, G. Martinez, and P. Wyder, Phys. Rev. B **60**, 4438 (1999).
[7] A. V. Rodina, M. Dietrich, A. Göldner, L. Eckey, A. Hoffmann, A. L. Efros, M. Rosen, and B. K. Meyer, Phys. Rev. B **64**, 115204 (2001).
[8] M. Sobol and W. Bardyszewski, Phys. Rev. B **73**, 075208 (2006).
[9] P. A. Shields, R. J. Nicholas, N. Grandjean, and J. Massies, Phys. Rev. B **63**, 245319 (2001).
[10] G. E. W. Bauer and T. Ando, Phys. Rev. B **38**, 6015 (1988).
[11] W. Bardyszewski and D. Yevick, Phys. Rev. B **49**, 5368 (1994).
[12] W. Bardyszewski, D. Yevick, Y. Liu, C. Rolland, and S. Bradshaw, J. Appl. Phys. **80**, 1136 (1996).
[13] W. Bardyszewski and S. P. Lepkowski, Phys. Rev. B **85**, 035318 (2012).
[14] S. L. Chuang and C. S. Chang, Phys. Rev. B **54**, 2491 (1996).
[15] S. P. Lepkowski, J. A. Majewski, and G. Jurczak, Phys. Rev. B **72**, 245201 (2005).
[16] J. Pal, G. Tse, V. Haxha, M. A. Migliorato, and S. Tomic, Phys. Rev. B **84**, 085211 (2011).
[17] W. E. Lamb-Jr, Phys. Rev. **85**, 259 (1952).
[18] A. Punya and W. R. L. Lambrecht, Phys. Rev. B **85**, 195147 (2012).
[19] N. Okamoto, K. Hoshino, N. Hara, M. Takikawa, and Y. Arakawa, J. Cryst. Growth **272**, 278 (2004).
[20] J. Pal, M. A. Migliorato, C.-K. Li, Y.-R. Wu, B. G. Crutchley, I. P. Marko, and S. J. Sweeney, J. Appl. Physics **114**, 073104 (2013).